



HAL
open science

Bio-Based Hybrid Magnetic Latex Particles Containing Encapsulated γ -Fe₂O₃ by Miniemulsion Copolymerization of Soybean Oil-Acrylated Methyl Ester and Styrene

Anderson Medeiros, Fabricio Machado, Elodie Bourgeat-lami, Joel Rubim, Timothy Frederick Llewellyn Mckenna

► To cite this version:

Anderson Medeiros, Fabricio Machado, Elodie Bourgeat-lami, Joel Rubim, Timothy Frederick Llewellyn Mckenna. Bio-Based Hybrid Magnetic Latex Particles Containing Encapsulated γ -Fe₂O₃ by Miniemulsion Copolymerization of Soybean Oil-Acrylated Methyl Ester and Styrene. *Macromolecular Materials and Engineering*, 2018, pp.1800449. 10.1002/mame.201800449 . hal-01980510

HAL Id: hal-01980510

<https://hal.science/hal-01980510>

Submitted on 12 Nov 2020

HAL is a multi-disciplinary open access archive for the deposit and dissemination of scientific research documents, whether they are published or not. The documents may come from teaching and research institutions in France or abroad, or from public or private research centers.

L'archive ouverte pluridisciplinaire **HAL**, est destinée au dépôt et à la diffusion de documents scientifiques de niveau recherche, publiés ou non, émanant des établissements d'enseignement et de recherche français ou étrangers, des laboratoires publics ou privés.

1 **Bio-based Hybrid Magnetic Latex Particles Containing Encapsulated**
2 **γ -Fe₂O₃ by Miniemulsion Copolymerization of Soybean Oil-Acrylated Methyl Ester and**
3 **Styrene**

4
5 Anderson M.M.S. Medeiros,^{1,2,#*} Fabricio Machado,³ Elodie Bourgeat-Lami,¹ Joel C. Rubim²
6 and Timothy F.L. McKenna^{1,*}

7
8 ¹ Université Claude Bernard Lyon 1, CPE Lyon, Laboratoire de Chimie Catalyse Polymères et
9 Procèdes (C2P2), LCPP Group, CNRS, UMR 5265, 43 Bvd. du 11 Novembre 1918, F-69612,
10 Villeurbanne, France. E-mail: timothy.mckenna@univ-lyon1.fr

11 ² Laboratório de Materiais e Combustíveis – LMC – Instituto de Química, Universidade de
12 Brasília, *Campus* Universitário Darcy Ribeiro, CP: 04478, CEP 70910-100, Brasília, Distrito
13 Federal, Brazil. E-mail: jocrubim@gmail.com or jocrubim@unb.br

14 ³ Laboratório de Desenvolvimento de Processos Químicos – LDPQ – Instituto de Química,
15 Universidade de Brasília, *Campus* Universitário Darcy Ribeiro, CP: 04478, CEP 70910-100,
16 Brasília, Distrito Federal, Brazil

17 _____

18

19 **Abstract:** This work reports the use of acrylated fatty acid methyl ester
20 (AFAME) as biomonomer for the synthesis of bio-based hybrid magnetic
21 particles poly(styrene-*co*-AFAME)/ γ -Fe₂O₃ produced by miniemulsion
22 polymerization. Poly(styrene-*co*-AFAME)/ γ -Fe₂O₃ can be tailored intended
23 for use in various fields by varying the content of AFAME. The strategy
24 employed was to encapsulate superparamagnetic iron oxide nanoparticles

1 (SPIONs) as γ -Fe₂O₃ into styrene/AFAME-based copolymer matrix. Raman
2 spectroscopy was employed to ensure the formation of the SPIONs
3 (γ -Fe₂O₃) obtained by co-precipitation technique followed by oxidation of
4 Fe₃O₄. The functionalization of SPIONs with oleic acid (OA) was carried
5 out to increase the SPIONs-monomer affinity. The presence of OA on the
6 surface of γ -Fe₂O₃ was certified by identification of main absorption bands
7 by FTIR. Thermal analysis (DTG/DTA and DSC) results of poly(styrene-
8 *co*-AFAME)/ γ -Fe₂O₃ showed an increase in AFAME content leading to a
9 lower copolymer T_g . DLS measurements resulted in poly(styrene-*co*-
10 AFAME)/ γ -Fe₂O₃ particles with diameter in the range of 100 to 150 nm. It
11 could also be observed by TEM and cryo-TEM techniques that γ -Fe₂O₃
12 particles were successfully encapsulated into the poly(styrene-*co*-AFAME)
13 matrix.

14
15 # This work is part of the PhD Thesis of Anderson M. M. S. Medeiros.

16 * Corresponding author: E-mail: timothy.mckenna@univ-lyon1.fr (T. F. L. McKenna)

19 1. Introduction

20
21 Superparamagnetic iron oxide nanoparticles (SPIONs) have aroused a great deal of interest
22 in industrial and academic research because of their intrinsic properties such as
23 superparamagnetism, high saturation magnetization, extra anisotropy contributions, negligible
24 residual magnetization and coercivity, and, low costs of production.^[1, 2] In this sense, these
25 materials can be employed in various fields such as paints ^[3, 4], high density magnetic

1 recording media ^[5], sensors and biosensors ^[6], catalyst supports ^[7] as well as in biological
2 applications ^[8, 9] and nanomedicine ^[10-15]. Furthermore, SPIONs can be combined with other
3 materials that have different properties, and they can generate new materials, referred to as
4 magnetic nanocomposites, which are very versatile with singular characteristics.

5 Magnetic nanocomposites have emerged as efficient way to upgrade structures already
6 established. For decades, magnetic hybrid nanomaterials consisting of a distribution of
7 magnetic nanoparticles (MNPs) in a polymeric matrix have been extensively studied in terms
8 of property improvements such as mechanical, ^[16] thermal, ^[17] electrical ^[18, 19] and optical
9 properties. ^[20-22]

10 Among the magnetic nanocomposites, those formed by a combination of magnetic and
11 polymer particles deserves special attention due to their great affinity with biological systems
12 and the ability to alter the variation of magnetic behavior under the action of magnetic
13 fields.^[23-27] The specialized literature reports several researches on the development of
14 magnetic nanocomposites using polymeric matrixes. Chen and co-authors described the
15 synthesis of a spherical polyelectrolyte brushes containing magnetic encapsulated
16 nanoparticles. According to the authors, the material is composed by polystyrene core-
17 incorporated magnetic nanoparticles and a brush shell formed by a linear poly(acrylic acid)
18 attached by covalent bonds to the core surface that was synthesized by photo-polymerization.
19 The authors affirm that this material can be employed in catalysis, wastewater treatment,
20 disease diagnosis and bio-engineering including enzyme immobilization and protein
21 adsorption, which represents the versatility of magnet-polymer materials.^[28]

22 Along the same line, Ferreira and co-workers reported the development of poly(vinyl
23 acetate)-embedded Fe₃O₄ nanospheres through batch suspension polymerization. The authors
24 have performed polymerization of vinyl acetate in the presence of MNPs. The incorporation
25 of MNPs into polymeric matrix occurred *in situ* and the material presents potential application

1 as device of intravascular embolization.^[29] In another example, magnetic polyurethanes (PU)
2 were synthesized and described by Einloft et al.^[30]. According to the authors, Fe₃O₄-synthetic
3 talc, obtained by addition of synthetic talc in the process of Fe₃O₄ synthesis, have been
4 frequently used as nanofiller reinforcement for polyurethanes. It was dispersed into the PU
5 matrix in order to improve the crystallization temperature and thermal stability. The presence
6 of magnetite as a filler indicated the reorganization of polyurethane structure and caused the
7 disappearance of spherulites, increasing the roughness. This phenomenon was explained by
8 the hydrogen bonding balance between polymer/polymer, polymer/filler and filler/filler.

9 A number of approaches have been described for the synthesis of iron oxide/polymer
10 nanocomposites, as for instance, conventional emulsion polymerization,^[31] soapless emulsion
11 polymerization,^[32, 33] inverse emulsion polymerization,^[34, 35] atom transfer radical
12 polymerization,^[36] or reversible addition fragmentation chain transfer polymerization.^[37, 38]
13 However, miniemulsion technique deserves especial attention due to the high potential to
14 encapsulate inorganic fillers, elevated colloidal stability, droplet nucleation, and the
15 possibility of using both water-soluble and organo-soluble initiators. According to
16 Landfester,^[39] miniemulsion process is a practical route to the tailor-made synthesis of
17 inorganic/polymer composite particles. The particle formation mechanism proper to
18 miniemulsion – the high content of monomer into droplet contributes to the low internal
19 viscosity and thus thermodynamic equilibrium is reached – is particularly advantageous for
20 making composite polymer particles and will be a main factor in controlling (e.g. as function
21 of surfactant concentration) the morphology and shape of the final products.^[40] Additionally,
22 mass transfer through aqueous phase is not necessarily required and the alternative of using
23 organo-soluble initiators is decisive, in cases of biobased polymers, since these raw materials
24 have low intrinsic reactivity.

1 The scientific literature reports researches involving the use of miniemulsion
2 polymerization for development of magnetic hybrid nanomaterials as, for instance, the
3 encapsulation of MNPs in poly(methyl methacrylate) (PMMA) through miniemulsion as
4 reported by Feuser et al.^{[41],[42]}. According to the research, the obtained nanocomposites with
5 ca. 100 nm average diameters did not present cytotoxicity, making them suitable for
6 application in hyperthermia treatment as suggested by the authors. Mahdavian et al.^[43] have
7 used miniemulsion polymerization in order to obtain encapsulated-iron oxide nanoparticles
8 into butyl acrylate/styrene copolymer. They reported the synthesis of magnetic composites
9 with high content of encapsulated iron oxide (almost 32% relative to the polymer amount). Li
10 and co-workers^[44] have developed a spherical caged superparamagnetic nanocomposite
11 (SCN) (polystyrene/Fe₃O₄@SiO₂) employing a combination of miniemulsion and sol-gel
12 techniques. The hybrid material, so-called yolk/shell nanocomposite (YSNs), was composed
13 of a polymeric core (polystyrene) and a magnetic-functionalized shell (Fe₃O₄@SiO₂).

14 Recently, researchers have turned their attention to the use of renewable sources in the
15 synthesis of magnetic nanocomposites due to eco-friendly politics and new socio-ecological
16 scenarios that have been established. Also, bio-based (co)polymers can have low cost in
17 certain cases, present biodegradability, biocompatibility and distinct properties when
18 compared to commercial polymers.^[45, 46]

19 Meiorin and co-authors^[47] have investigated the effect of incorporation of Fe₃O₄ MNPs
20 into copolymers composed by styrene/tung oil (China wood oil). As explained by the authors,
21 the incorporation of MNPs stiffened the material and reduced the ultimate strain,
22 consequently, increasing its fragility. Medeiros and co-workers^[48] have developed a bio-based
23 nanocomposite consisting of a maghemite (γ -Fe₂O₃) dispersion into a fatty acid-matrix
24 [poly(AFACO)] from castor oil. It was shown that the strategy adopted of modifying the
25 surface of MNPs with acrylated-fatty acid from castor oil (AFACO) may lead to an increase

1 in the affinity between $\gamma\text{-Fe}_2\text{O}_3$ and the polymer from raw material, allowing for proper MNPs
2 dispersion and reducing the probability of MNPs leaching. In the same vein, Peres et al. [49]
3 described a new route to develop a magnetic polyester from castor oil. The results reached by
4 the researchers suggest that the new material presented good thermal stability and behaves as
5 superparamagnetic material.

6 Considering this context, the present work describes the development of a new class of
7 polymeric materials based on vegetable oil. Vegetable oils had been employed to modify
8 conventional properties of polystyrene and encapsulated MNPs providing magnetic properties
9 to the new material. We will thus examine the encapsulation of $\gamma\text{-Fe}_2\text{O}_3$ by copolymers based
10 on soybean oil acrylated-methyl ester (AFAME) and styrene using miniemulsion
11 polymerization. For this purpose, methyl ester was obtained and modified in two steps
12 (epoxidation followed by ring-opening with acrylic acid). In addition, $\gamma\text{-Fe}_2\text{O}_3$ SPIONs were
13 synthesized by co-precipitation method and their surface was functionalized with oleic acid
14 (OA) (hereafter referred to as $\gamma\text{-Fe}_2\text{O}_3\text{@OA}$) for increasing MNP-monomer and MNPs-
15 polymer interactions. Our interest to use $\gamma\text{-Fe}_2\text{O}_3$ rather than Fe_3O_4 is basically due to high
16 chemical stability of $\gamma\text{-Fe}_2\text{O}_3$. Considering that maghemite is an iron oxide, which has only
17 Fe^{3+} , these SPIONs will not lose chemical stability due to oxidation reaction. In other hand,
18 the magnetite, Fe_3O_4 , could be oxidized to $\gamma\text{-Fe}_2\text{O}_3$, which might generate an unstable
19 polymer latex. Nanoparticles of magnetic poly(styrene-*co*-AFAME)/ $\gamma\text{-Fe}_2\text{O}_3$ were obtained
20 with different AFAME content. SPIONs and SPIONs@OA were characterized by Raman
21 spectroscopy, X-ray diffraction, transmission electronic microscope (TEM), FTIR, TGA and
22 SQUID magnetic measurements. Poly(styrene-*co*-AFAME)/ $\gamma\text{-Fe}_2\text{O}_3$ properties were
23 evaluated by FTIR, TEM and cryo-TEM, TGA, DSC-DTA and magnetization measurements.

24

25

2. Experimental Section

2.1 Chemicals

The analytical-grade reagents NaOH ($\geq 98\%$, Sigma-Aldrich), FeCl₂·4H₂O (Sigma-Aldrich), FeCl₃·6H₂O (Sigma-Aldrich), ethanol (99%, LAURYLALAB), acetone (99%, LAURYLALAB), methanol (99%, LAURYLALAB), HNO₃ (68-70%, Sigma-Aldrich) soybean oil (Sigma-Aldrich), formic acid (SIGMA-ALDRICH), H₂O₂ (35%) (ACROS-ORGANICS), diethyl ether (Sigma-Aldrich), 1,2-dichloroethane (Sigma-Aldrich), NaHCO₃ (ACROS-ORGANICS), acrylic acid (Sigma-Aldrich), Sodium dodecyl sulfate (SDS) ($\geq 99\%$, Sigma-Aldrich) hexadecane (FISHER-SCIENTIFIC) and hydroquinone (99%, ACROS-ORGANICS) were used as obtained. Styrene (Sigma-Aldrich) and 2,2'-azobis (2-methylpropionitrile) (AIBN) ($> 98\%$, Sigma-Aldrich) were used without purification.

2.2 Synthesis and Characterization

Synthesis of γ -Fe₂O₃: Maghemite was obtained by the co-precipitation method followed by chemical oxidation using concentrated HNO₃.^[50] Firstly, 125 mL of an acid solution containing Fe²⁺ (0.09 mol·L⁻¹) and Fe³⁺ (0,18 mol·L⁻¹) (Fe(II):Fe(III) stoichiometric ratio of 1:2) was prepared by dissolution of FeCl₂ and FeCl₃ in distilled water, then heating the solution to 60 °C. 625 mL of 2M NaOH solution was prepared in a 2 L beaker, and then heated to 60 °C under mechanical vigorous stirring. When both solutions reached thermal equilibrium, the iron solution was added to the alkali solution very quickly and kept for one hour under vigorous stirring. The black precipitate formed was separated using a neodymium magnet and was washed three times with each solvent, distilled water, ethanol and acetone,

1 respectively. Then, the black precipitate was kept in contact with 150 mL of concentrated
2 HNO₃ (2M) for 1 h. The brownish precipitate obtained was separated with a neodymium
3 magnet and was further washed with acetone. At the end, around 20 g of γ -Fe₂O₃ was
4 obtained.

5 Synthesis of modified γ -Fe₂O₃@OA: 5g of brownish SPIONs were re-dispersed in 170 mL of
6 an acidic aqueous solution and kept under vigorous mechanical stirring. The system was
7 heated up to 75 °C, followed by dropwise addition of oleic acid (5 mL) to the SPIONs
8 dispersion. The mixture was kept under stirring for 2 h after which two phases were observed
9 (water and oil-SPIONs). With a magnet, the SPIONs phase was separated and washed several
10 times with ethanol and acetone.

11 Synthesis of acrylated fatty acid methyl ester (AFAME) from Soybean Oil: Basically,
12 AFAME was synthesized following three main steps (see Figure 1): **i**) the first one is
13 characterized by the formation a fatty acid methyl ester (FAME) through the reaction between
14 soybean oil (100 g) and methanol (1:6 oil to alcohol ratio, respectively) in presence of sodium
15 hydroxide (1 wt%) as basic catalyst for three hours. It is important to note that an excess of
16 methanol was employed to ensure the complete transesterification and to avoid the
17 equilibrium shift in the reverse direction. The final reaction product was purified with distilled
18 water, sodium bicarbonate, followed by filtration by using a basic alumina column^[51]; **ii**) the
19 second step consisted in the epoxidation reaction of 50 g of FAME carried out with a mixture
20 containing a molar ratio of 1/4/2 (FAME/1,2-dichloroethane and formic acid, respectively) in
21 a 250 mL three-neck round-bottom flask under vigorous magnetic stirring. When the the
22 system reached thermal equilibrium at 45 °C, hydrogen peroxide (35%) (molar ratio of
23 FAME/H₂O₂ was 1/20) was added dropwise during one hour and the reaction was performed
24 for 16 h, followed by extraction of the epoxidized FAME (EFAME) with diethyl ether. The
25 EFAME was then washed with distilled water and treated with sodium bicarbonate solution

1 until alkali pH was obtained and the conversion was ca. 96%;^[52] **iii)** the last step comprises
2 the oxirane ring opening reaction performed in a 250 mL three-neck round-bottom flask at 75
3 °C. Initially, a mixture consisting of acrylic acid and hydroquinone (molar ratio of 6/3.5x10⁻²
4 of acrylic acid/hydroquinone, respectively) at 75 °C was added very slowly to the EFAME
5 (50 g) and kept under vigorous magnetic stirring for 8 h. The reaction product, acrylated fatty
6 acid methyl ester (AFAME), was purified following the same experimental procedure
7 described for EFAME purification.^[53] The experimental procedure was similar to the one
8 described by Medeiros et al.,^[54] and the reader is referred to this publication for a more
9 detailed description of the protocol. The overall conversion was ca. 93%.

10

11 Figure 1. Representative schema of the reaction steps involved in the AFAME synthesis.

12

13 γ -Fe₂O₃@OA monomer dispersion: SPIONs@OA was dispersed in styrene and the magnetic
14 fluid (MF) was kept in ultrasound bath for 2 h. The aggregates of maghemite (coarse
15 particles) were removed by centrifugation and a stable magnetic suspension with 20% of solid
16 content was accomplished.

17 Pre-emulsification: In all the systems, 10 g of oil-phase was used, even with the variation of
18 AFAME. An appropriate amount of AFAME [5%, 25% or 50% (wt/wt)] was introduced in
19 the oil-phase (containing γ -Fe₂O₃@OA dispersed in styrene) and the mixture was
20 homogenized for 24 h. Then, the required amounts of AIBN (2 wt%) and hexadecane (6 wt%)
21 were added and the system was kept under stirring for 30 min. Simultaneously, 40 g of
22 aqueous phase containing 0.1 g of dissolved SDS was homogenized for 30 min. Then, the oil-
23 phase was added to the aqueous solution and the mixture was kept for 1 h under vigorous

1 stirring. Table 1 shows the loadings of chemicals used to perform four (4) different
2 miniemulsion polymerization reactions.

3

4 Table 1

5

6 Miniemulsion polymerization: After emulsification of the AFAME containing oil phase, a
7 nanosize dispersion was generated by ultrasonication of the pre-emulsion for 120 s at 70%
8 amplitude (VCX SONICS 750W) at 0 °C in order to prevent polymerization. Finally, the
9 reaction of polymerization was conducted at 75 °C for 4h. This process is represented in the
10 schema of Figure 2.

11

12 Figure 2. Schema of the miniemulsion polymerization process.

13

14 Characterizations: X-ray diffraction (XRD) patterns from SPIONs were obtained using a
15 Bruker AXS D8 FOCUS XRD instrument with the generator operating at 40 mA and 30 kV,
16 with Cu K α radiation ($\lambda = 1.5406 \text{ \AA}$) selected by a graphite monochromator.

17 Raman analyses were performed on a Labram HR800 spectrograph (Jobin Yvon-Horiba).
18 The Raman spectra were excited at 514.5 nm (Ar⁺/Kr⁺ laser from Spectra Physics). The
19 Raman signal of a Si wafer at 520.7 cm⁻¹ was used to calibrate the instrument. The laser
20 power on the sample was adjusted to avoid sample decomposition.

21 The presence of oleic acid on SPIONs surface was investigated by Fourier Transform
22 Infrared (FTIR) spectroscopy on a Shimadzu IR-Prestige 21 system using an attenuated total
23 reflectance (ATR) cell (MIRacle from PIKE Technologies) with a diamond prism. Each FTIR
24 spectrum is the result of 32 scans at a nominal resolution of 4 cm⁻¹.

1 Thermogravimetric measurements were acquired on a Shimadzu TG-60 system. During
2 scanning, the system was purged with N₂ at a rate of 50 mL·min⁻¹. The average sample
3 weight was 10 mg, and a temperature ramp from 25 °C to 800 °C was applied at a heating rate
4 of 10 °C·min⁻¹. Differential Scanning Calorimetry (DSC) was carried out on a DSC 131
5 Setaram device. The samples were heated from -30 to 120 °C with a heating rate of
6 10 °C·min⁻¹ for three times and the second heating runs were used for analysis.

7 Dynamic Light Scattering (DLS) measurements were performed in a Nano Zetasizer
8 Malvern. The diluted latex was kept in a glass cuvette and triplicate analyses were performed.

9 Transmission electron microscopy (TEM) was performed on a Philips CM120 electron
10 microscope operating at an accelerating voltage of 100 kV. The samples were prepared by
11 drying a drop of sample onto carbon-coated copper grids covered by Formvar thin films (Ted
12 Pella, Inc.). Soft samples required the cryo-TEM technique.

13 Magnetic measurements were carried out using a Superconducting Quantum Interference
14 Device magnetometer (SQUID) from ADE Magnetics (Model EV7), operating at a
15 vibrational frequency of 75 Hz. The hysteresis loops (M vs H) of the samples were acquired
16 under applied magnetic fields varying from -50 kOe to +50 kOe at 300 K.

17

18 **3. Results and Discussion**

19

20 **3.1 SPIONs (γ -Fe₂O₃ and γ -Fe₂O₃@OA)**

21

22 The γ -Fe₂O₃ and its precursor, Fe₃O₄, were characterized by Raman spectroscopy, as
23 displayed in Figure S1 (Supporting Information). According to Shebanova and Lazor^[55, 56]
24 magnetite belongs to the octahedral group and five Raman active phonons are expected with
25 a_{1g} + e_g + 3t_{2g} symmetries. In this sense, the features observed in the Raman spectrum of

1 Figure S1a (magnetite) at 190 (t_{2g}), 310 (e_g), 532 (t_{2g}) and 664 cm^{-1} (a_{1g}) are the Raman
2 signature of magnetite. The broad Raman signals (see Figure S1b) observed at 358, 490,
3 690 cm^{-1} are characteristic of $\gamma\text{-Fe}_2\text{O}_3$,^[57, 58] the SPIONs used in the development of this
4 work.

5 The average diameters of the magnetic nanoparticles were determined based on the TEM
6 micrograph images of $\gamma\text{-Fe}_2\text{O}_3$ and $\gamma\text{-Fe}_2\text{O}_3\text{@OA}$ nanoparticles (Figure S2 – Supporting
7 information) and XRD measurements (Figure S3 – Supporting information). TEM results
8 showed that the $\gamma\text{-Fe}_2\text{O}_3$ and $\gamma\text{-Fe}_2\text{O}_3\text{@OA}$ nanoparticles are nearly spherical, presenting a
9 homogenous size distribution with mean diameters of 7.1 nm and 7.0 nm, respectively. .

10 The crystalline structure of SPIONs was analyzed by powder XRD. A comparison of the
11 XRD results displayed in Figure S3 (Supporting Information) with those of the XRD pattern
12 of a spinel cubic structure (JCPDS N° 77-0435) confirms that the obtained SPIONs have a
13 similar crystalline structure. The XRD pattern is also in agreement with JCPDS data for
14 maghemite (Card N° 39-1346).

15 Based on Figure S3, and employing the Debye-Scherrer^[59] equation, the calculated
16 average diameters of $\gamma\text{-Fe}_2\text{O}_3$ and $\gamma\text{-Fe}_2\text{O}_3\text{@OA}$ were 6.3 and 6.5 nm, respectively, showing a
17 reasonable agreement with TEM results.

18 The presence of oleic acid/oleate on the surface of maghemite was investigated by FTIR-
19 ATR as shown in Figure 3.

20

21 Figure 3. FTIR-ATR spectra of: (a) oleic acid, (b) $\gamma\text{-Fe}_2\text{O}_3$, and (c) $\gamma\text{-Fe}_2\text{O}_3\text{@OA}$.

22

23 Table 2

24

25

1 In the IR spectrum of γ -Fe₂O₃ (Figure 3b), it is possible to identify characteristic
2 absorption bands at 573 and 3400 cm⁻¹, attributed to the Fe-O and O-H stretching modes of
3 γ -Fe₂O₃ and physisorbed H₂O molecules, respectively [60]. The OH bending at 1624 cm⁻¹ can
4 be also observed in Figure 3b and it may be associated to bulk OH in iron oxyhydroxides
5 present on the surface of γ -Fe₂O₃ [61]. In the spectrum of γ -Fe₂O₃@OA (Figure 3c) besides the
6 vibrational modes observed in Figure 3b, other absorption bands are observed at 1415, 1517,
7 1722, 2890, 2930 and 3010 cm⁻¹ that are absent in spectrum of Figure 3b (see Table 2). These
8 features are assigned to the oleic acid/oleate [62].

9 According to Nakamoto [63], the difference (Δ) in the wavenumbers associated to the
10 carboxylate symmetric and asymmetric stretching modes [$\Delta = (\nu_{as}(\text{COO}^-) - \nu_s(\text{COO}^-))$]
11 indicates the type of carboxylate coordination as depicted in Figure 4. In the present case the
12 obtained Δ value was 102 cm⁻¹ suggesting that the carboxylate moiety interacts with the
13 SPIONs surface as depicted in Figure 4c.

14

15 Figure 4. Types of metal-carboxylate coordination: (a) Bridging, (b) unidentate, and (c)
16 chelating bidentate.

17

18 In order to estimate the quantity of oleic acid present on the surface of SPIONs,
19 thermogravimetric measurements were performed and the results are shown in Figure 5.

20

21 Figure 5. Thermograms of (a) γ -Fe₂O₃ and (b) γ -Fe₂O₃@OA.

22

23 In agreement with the FTIR measurements, the thermogram of γ -Fe₂O₃@OA indicates the
24 presence of an organic phase (oleic acid) on the maghemite's surface. Comparing the
25 thermograms in Figure 5, one can assume that the observed weight loss (20%) is attributed to

1 OA degradation, since the $\gamma\text{-Fe}_2\text{O}_3$ shows a great thermal stability (see thermogram in
2 Figure 5 (a)). To evaluate the OA surface coverage, we have considered the following data: **i)**
3 the amounts of SPIONs ($\gamma\text{-Fe}_2\text{O}_3$) and OA as obtained from the thermograms; **ii)** it was
4 assumed that the SPIONs are spherical with an average diameter (d) of 6,3 nm as determined
5 by XRD ; **iii)** the density of maghemite, ρ , as $4.9 \text{ g}\cdot\text{cm}^{-3}$ [64]; **iv)** the molar mass (MM) of OA
6 as $282.5 \text{ g}\cdot\text{mol}^{-1}$) and **v)** it was assumed that each OA molecule occupies 1 nm^2 of surface
7 area. With these data, we estimate the total surface area of SPIONs (A_{SPIONs}) and the total area
8 occupied by OA molecules (A_{OA}) using the equations shown in the Supporting Information.
9 Considering the obtained ratio $A_{\text{OA}}/A_{\text{SPIONs}}$, we can assume that the SPIONs surface is
10 covered by approximately 3 monolayers of OA.

11

12 Table 3

13

14 The magnetic response of maghemite was evaluated by magnetization measurements. The
15 data were recorded at 300 K and the results presented in Figure 6 showed a saturation
16 magnetization (M_s) of $57 \text{ emu}\cdot\text{g}^{-1}$ and agrees with previous literature data for bulk
17 maghemite^[65]. It shows also negligible coercivity and remanent magnetization. Considering
18 these properties, $\gamma\text{-Fe}_2\text{O}_3$ displays superparamagnetic behavior.

19

20 Figure 6. Hysteresis loop of $\gamma\text{-Fe}_2\text{O}_3$ recorded at 300 K. The inset shows an expanded view of
21 the magnetization curve.

22

23

24

25

1 **3.2 Encapsulation of SPIONs (γ -Fe₂O₃) by Miniemulsion Polymerization**

2

3 The polymer-encapsulated SPIONs were prepared by miniemulsion polymerization using
4 four different compositions of monomeric phase (styrene and AFAME) as shown in Table 1,
5 in order to study the effect of reaction conditions on the properties of the resulting materials.
6 The hydrodynamic diameter (Z-average) of the encapsulated iron oxide particles was
7 evaluated by DLS as shown in Figure 7 and Table 4.

8

9 Figure 7. Size distribution curves of poly(styrene-*co*-AFAME)/ γ -Fe₂O₃ composite latex
10 particles of various styrene/AFAME ratios as determined by DLS. See Table 1 for detailed
11 experimental conditions.

12

13 Table 4

14

15 Figure 7 shows that a unimodal particle size distribution is observed for all systems, from
16 low to higher AFAME contents and this behavior was verified throughout the reactions. This
17 implies that there was no significant Ostwald ripening or coalescence and that a stable colloid
18 system was obtained each time. Previous research published by our group shows that the
19 concentration of AFAME had an important influence on the kinetic of the overall
20 conversion.^[54] In agreement with Laurentino et. al.,^[66] the research displays that increasing
21 the AFAME concentration caused a decrease on the overall conversion because the kinetic
22 rate of both monomers are expected to be quite different. Furthermore, based on Table 4 it can
23 be noted that the average particle size slightly increased in cases of high AFAME content.
24 The increase in the particle size is attributed to the high viscosity of AFAME that can turn
25 more difficult the shearing process during the ultrasonication stage.

1 TEM and cryo-TEM images of the encapsulated SPIONs presented in Figure 8 show
2 particles with spherical morphology and demonstrate very clearly the proper encapsulation of
3 the SPIONs by the copolymer. Note also that these images suggest a relatively narrow particle
4 size distribution that is coherent with DLS measurements.

5
6 Figure 8. (a, b) TEM and (c, d) cryo-TEM images of poly(styrene-*co*-AFAME)/ γ -Fe₂O₃
7 composite particles for different compositions. Styrene/AFAME (wt%/wt%) = 100/0 (a), 95/5
8 (b), 75/25 (c) and 50/50 (d). See Table 1 for detailed experimental conditions.

9
10 The images in Figure 8 show particles sizes of approximately 92, 90, 102, 97 nm,
11 respectively, for systems containing styrene:AFAME ratios of 100/0, 95/5, 75/25 and 50/50
12 (wt%). The particles sizes determined by TEM and cryo-TEM are smaller than those ones
13 obtained by DLS since the particle size given by DLS is determined in terms of the
14 hydrodynamics radius. According to Figure 8, as the mass fraction of AFAME is increased
15 the amount of SPIONs dispersed into the copolymer matrix is decreased, which reflects the
16 low compatibility between SPIONs@OA and AFAME.

17 The quantity of SPIONs effectively incorporated into the polymer particles was determined
18 by TGA and the obtained thermograms are depicted in Figure S4 (Supporting Information).

19 The thermograms of encapsulated-SPIONs showed a profile similar to those that had no
20 SPIONs incorporated. However, the curves of magnetic polymers showed a residual mass
21 higher than the non-magnetic polymer. This mass difference is due to the thermally and
22 chemically stable SPIONs.

23 Comparing each thermogram of magnetic and non-magnetic polymers (see Figure S4), it
24 can be estimated that nearly 6% of SPIONs were encapsulated by the
25 poly(styrene-*co*-AFAME) copolymer. These thermograms also show that the incorporation of

1 γ -Fe₂O₃ decreased with increasing AFAME content. This behavior may be explained by the
2 low affinity between SPIONs@OA and AFAME since the presence of the incorporated
3 acrylate group increases the polar behavior of AFAME while oleic shell on the SPIONs
4 surface shows a non-polar nature. These results are in agreement with the TEM
5 measurements, since a decrease of the amount of SPIONs in the copolymer was observed with
6 increasing the AFAME content.

7 DSC/DTA analyses were performed in order to obtain the glass transition temperatures
8 (T_g) of magnetic copolymers and the values are shown in Table 5.

9

10 Table 5

11

12 First of all, it is important to mention that the presence of only one glass transition
13 temperature confirms the production of copolymers. The experimental results portrayed in
14 Table 5 clearly show that the T_g of samples with low AFAME content are higher than those
15 with high AFAME content. This effect was expected because polymers based on vegetable
16 oils have normally low glass transitions.^[67] However, comparing the samples containing
17 magnetic particles with their pure polymer counterparts, it is possible to see that the T_g of all
18 the magnetic samples are higher than the non-magnetic copolymers. This behavior indicates
19 that the presence of SPIONs into the copolymer promotes an increase of hardness and
20 suggests an interaction between the SPIONs and the copolymer matrix.^[47]

21 The magnetic behavior of the investigated materials is shown in Figure 9 and the
22 corresponding values of magnetization saturation (M_s), remanence (M_r) and coercivity (H_c)
23 are displayed in Table 6.

24

1 Figure 9. Hysteresis loop at 300 K of (a) polystyrene, (b) poly(AFAME) and (c-e)
2 poly(styrene-co-AFAME)/ γ -Fe₂O₃ composite latex suspensions of various compositions.
3 Styrene/AFAME (wt%/wt%) = 50/50 (c), 75/25 (d) and 95/5 (e). See Table 1 for detailed
4 experimental conditions. The inset shows an amplified region close to zero applied fields.

5

6 Table 6

7

8 The negligible values of remanence and coercivity suggest that the materials present a
9 superparamagnetic behavior. In addition, the increase in the AFAME content reveals a
10 decrease in the copolymer magnetic response as consequence of a decrease in the
11 incorporation of SPIONs in the copolymer matrix, which was demonstrated by the TGA data
12 (Figure S4 – Supporting Information) and cryo-TEM images (Figure 8) and cryo-TEM
13 images (Figure 8).

14 As shown in Figure 6, the magnetic response of the bulk maghemite was 57 emu.g⁻¹.
15 Compared to bulk maghemite, the magnetic response of the poly(styrene-co-AFAME)/ γ -
16 Fe₂O₃ was reduced to 41.5, 31.5, and 26.2 emu.g⁻¹. This effect is mainly caused by the
17 decreasing of the presence of SPIONs into the polymeric structure. Considering also the
18 nanosized particles, the surface effect is critical for the magnetic behavior. It is believed the
19 interactions between polymeric fraction (a magnetically dead layer) and SPIONs-surface
20 might contribute to the reduction because this exchange serves to pin the magnetic
21 contribution of the surface without adding additional magnetization to the system.^[68]

22

23 Figure 10. Photos of dried poly(styrene-co-AFAME)/ γ -Fe₂O₃ with ratio (A) 100/0, (B) 95/5
24 (C) 75/25 and (D) 50/50, in absence and presence of a Nd magnet.

25

1 It is noteworthy that the images of the samples of magnetic polymers shown in Figure 10
2 were resulted by drying of a small part of obtained latex at the end of polymerization. These
3 images show a magnetic behavior of poly(styrene-*co*-AFAME)/ γ -Fe₂O₃ for all copolymer
4 compositions as well as the different macroscopic aspects among the polymers as
5 characterized by DSC. As listed in Table 5, as increase of AFAME amount as decrease the T_g ,
6 the polymer will be consequently softer and more flexible. Thus, poly(styrene-*co*-AFAME)/ γ -
7 Fe₂O₃ with higher amounts of AFAME can be applied in coatings and resins fields as well as
8 those one with low AFAME ratio could be used as embolic agent, for example.

10 4. Conclusion

11 Bio-based poly(styrene-*co*-AFAME)/ γ -Fe₂O₃ magnetic particles with styrene/AFAME
12 initial weight ratios of 100/0, 95/5, 75/25 and 50/50 were obtained by miniemulsion
13 polymerization. To promote the proper dispersion of SPIONs in AFAME comonomer, the
14 strategy used was to modify γ -Fe₂O₃ MNP with OA. TGA analysis showed that the modified
15 γ -Fe₂O₃ MNPs are covered by ca. 3 monolayers of OA and present superparamagnetic
16 behavior.

17 The poly(styrene-*co*-AFAME)/ γ -Fe₂O₃ composite particles have an average diameter of
18 120 – 150 nm, depending on the styrene:AFAME weight ratio. The larger particles were those
19 with higher AFAME content. In addition, TEM confirmed that the SPIONs were successfully
20 incorporated into the copolymer latex particles. The encapsulation of the SPIONs by the
21 copolymer matrix led to an increase in the T_g suggesting an increase in the hardness of the
22 bio-based magnetic material in comparison to the non-magnetic ones.

23 The poly(styrene-*co*-AFAME)/ γ -Fe₂O₃ bio-based magnetic particles, preserved the
24 superparamagnetic characteristics of the original modified SPIONs.

1 Additionally, it was observed that the based-AFAME copolymer can be used in a sort of
2 fields because it has different properties (e.g. glass transition temperature) depending on
3 AFAME content.

4 5 **Acknowledgments**

6
7 The authors thank Coordenação de Aperfeiçoamento de Pessoal de Nível Superior (CAPES),
8 Conselho Nacional de Pesquisa e Desenvolvimento (CNPq), and Fundação de Apoio à
9 Pesquisa do Distrito Federal (FAP-DF) for financial support and scholarships.

10
11 **Keywords:** bio-based; hybrid; copolymer; γ -Fe₂O₃; miniemulsion.

12 13 **5. References**

- 14
15 [1] R. H. Kodama, *J Magn Magn Mat* **1999**, *200*, 359.
16 [2] G. G. Nedelcu, A. Nastro, L. Filippelli, M. Cazacu, M. Iacob, C. O. Rossi, A. Popa, D.
17 Toloman, M. Dobromir, F. Iacomì, *Appl Surf Sci* **2015**, *352*, 109.
18 [3] P. Tiberto, G. Barrera, F. Celegato, M. Coisson, A. Chiolerio, P. Martino, P. Pandolfi, P.
19 Allia, *Eur. Phys. J. B* **2013**, *86*, 1.
20 [4] Z. Kaiyuan, W. N. Allen, M. Sinani, C. Martinez, D. Peroulis, "Magnetic nanoparticle ink
21 for RF integrated inductor applications", in *Microwave Symposium (IMS), 2014 IEEE MTT-S*
22 *International*, 20141.
23 [5] S. Giri, G. Pradhan, N. Das, *J Polym Res* **2014**, *21*, 1.
24 [6] T. A. P. Rocha-Santos, *TRAC-Trends in Analytical Chemistry* **2014**, *62*, 28.
25 [7] L. M. G. Rossi, M.A.S.; Vono, L.L.R.;, *J. Braz. Chem. Soc.* **2012**, *23*, 1959.
26 [8] N. C. Feitoza, T. D. Gonçalves, J. J. Mesquita, J. S. Menegucci, M.-K. M. S. Santos, J. A.
27 Chaker, R. B. Cunha, A. M. M. Medeiros, J. C. Rubim, M. H. Sousa, *The Journal of*
28 *Hazardous Materials* **2014**, *264*, 153.
29 [9] R. Lakshmanan, M. Sanchez-Dominguez, J. A. Matutes-Aquino, S. Wennmalm, G.
30 Kuttuva Rajarao, *Langmuir* **2014**, *30*, 1036.
31 [10] C. Xu, S. Sun, *Adv Drug Deliver Rev* **2013**, *65*, 732.
32 [11] R. Ladj, A. Bitar, M. M. Eissa, H. Fessi, Y. Mugnier, R. Le Dantec, A. Elaissari, *Int J*
33 *Pharm* **2013**, *458*, 230.
34 [12] M. K. Lima-Tenório, E. A. Gómez Pineda, N. M. Ahmad, H. Fessi, A. Elaissari, *Int J*
35 *Pharm* **2015**, *493*, 313.
36 [13] A. K. Hauser, R. J. Wydra, N. A. Stocke, K. W. Anderson, J. Z. Hilt, *J Control Release*
37 **2015**, *219*, 76.
38 [14] N. Lee, T. Hyeon, *Chem Soc Rev* **2012**, *41*, 2575.

- 1 [15] X. Chenjie, M. Luye, R. Isaac, M.-N. David, N. Matthias, A. A. James, Z. Weian, M. K.
2 Jeffrey, *Nanotechnol* **2011**, *22*, 1.
- 3 [16] J.-J. Luo, I. M. Daniel, *Compos Sci Technol* **2003**, *63*, 1607.
- 4 [17] H.-L. Tyan, Y.-C. Liu, K.-H. Wei, *Chem Mat* **1999**, *11*, 1942.
- 5 [18] H. C. Leventis, S. P. King, A. Sudlow, M. S. Hill, K. C. Molloy, S. A. Haque, *Nano Lett*
6 **2010**, *10*, 1253.
- 7 [19] E. Holder, N. Tessler, A. L. Rogach, *J Mat Chem* **2008**, *18*, 1064.
- 8 [20] R. J. Nussbaumer, W. R. Caseri, P. Smith, T. Tervoort, *Macromol Mat Eng* **2003**, *288*,
9 44.
- 10 [21] I. Armentano, M. Dottori, E. Fortunati, S. Mattioli, J. M. Kenny, *Polym Degrad Stabil*
11 **2010**, *95*, 2126.
- 12 [22] C. L. Sanchez, B.; Chaput, F.; Boilot, J.-P.;, *Adv. Mater.* **2003**, *15*, 1969.
- 13 [23] J. Ban, K. Kim, H. Jung, S. Choe, *J Ind Eng Chem* **2010**, *16*, 1040.
- 14 [24] T. S. Anirudhan, P. L. Divya, J. Nima, *Mat Sci Eng C* **2015**, *55*, 471.
- 15 [25] V. Chiaradia, A. Valério, P. E. Feuser, D. d. Oliveira, P. H. H. Araújo, C. Sayer, *Colloid*
16 *Surface A* **2015**, *482*, 596.
- 17 [26] A. Aqil, S. Vasseur, E. Duguet, C. Passirani, J. P. Benoît, A. Roch, R. Müller, R. Jérôme,
18 C. Jérôme, *Eur Polym J* **2008**, *44*, 3191.
- 19 [27] G. A. Kloster, D. Muraca, C. Meiorin, K. R. Pirota, N. E. Marcovich, M. A. Mosiewicki,
20 *Eur Polym J* **2015**, *72*, 202.
- 21 [28] K. Chen, Y. Zhu, Y. Zhang, L. Li, Y. Lu, X. Guo, *Macromol* **2011**, *44*, 632.
- 22 [29] G. R. Ferreira, T. Segura, F. G. de Souza Jr, A. P. Umpierre, F. Machado, *Eur Polym J*
23 **2012**, *48*, 2050.
- 24 [30] L. M. dos Santos, R. Ligabue, A. Dumas, C. Le Roux, P. Micoud, J.-F. Meunier, F.
25 Martin, S. Einloft, *Eur Polym J* **2015**, *69*, 38.
- 26 [31] X. Xu, G. Friedman, K. D. Humfeld, S. A. Majetich, S. A. Asher, *Chem Mat* **2002**, *14*,
27 1249.
- 28 [32] S. Sacanna, A. P. Philipse, *Langmuir* **2006**, *22*, 10209.
- 29 [33] K. Li, P. Y. Dugas, M. Lansalot, E. Bourgeat-Lami, *Macromolecules* **2016**, doi:
30 10.1021/acs.macromol.6b01546.
- 31 [34] R. Y. Hong, B. Feng, G. Liu, S. Wang, H. Z. Li, J. M. Ding, Y. Zheng, D. G. Wei, *J*
32 *Alloy Compd* **2009**, *476*, 612.
- 33 [35] Y. Chen, Z. Qian, Z. Zhang, *Colloid Surface A* **2008**, *312*, 209.
- 34 [36] Y. Wang, X. Teng, J.-S. Wang, H. Yang, *Nano Lett* **2003**, *3*, 789.
- 35 [37] K. Li, P.-Y. Dugas, E. Bourgeat-Lami, M. Lansalot, *Polymer* **2016**, doi:
36 10.1016/j.polymer.2016.07.087.
- 37 [38] D. Nguyen, B. T. T. Pham, V. Huynh, B. J. Kim, N. T. H. Pham, S. A. Bickley, S. K.
38 Jones, A. Serelis, T. Davey, C. Such, B. S. Hawkett, *Polymer* **2016**, doi:
39 10.1016/j.polymer.2016.08.064.
- 40 [39] M. Antonietti, K. Landfester, *Prog Polym Sci* **2002**, *27*, 689.
- 41 [40] J. M. Asua, *Prog Polym Sci* **2002**, *27*, 1283.
- 42 [41] P. E. Feuser, L. d. S. Bubniak, M. C. d. S. Silva, A. d. C. Viegas, A. Castilho Fernandes,
43 E. Ricci-Junior, M. Nele, A. C. Tedesco, C. Sayer, P. H. H. de Araújo, *Eur Polym J* **2015**, *68*,
44 355.
- 45 [42] P. E. Feuser, A. C. Fernandes, M. Nele, A. d. C. Viegas, E. Ricci-Junior, A. C. Tedesco,
46 C. Sayer, P. H. H. de Araújo, *Colloid Surface B* **2015**, *135*, 357.
- 47 [43] A. R. Mahdavian, Y. Sehri, H. Salehi-Mobarakeh, *Eur Polym J* **2008**, *44*, 2482.
- 48 [44] T. Li, X. Han, Y. Wang, F. Wang, D. Shi, *Colloid Surface A* **2015**, *477*, 84.
- 49 [45] X. Yang, S. Zhang, W. Li, *Prog Org Coat* **2015**, *85*, 216.
- 50 [46] S. Miao, P. Wang, Z. Su, S. Zhang, *Acta biomat* **2014**, *10*, 1692.

- 1 [47] C. Meiorin, D. Muraca, K. R. Pirota, M. I. Aranguren, M. A. Mosiewicki, *Eur Polym J*
2 **2014**, 53, 90.
- 3 [48] A. M. M. S. Medeiros, F. Machado, J. C. Rubim, *Eur Polym J* **2015**, 71, 152.
- 4 [49] E. U. X. Péres, F. G. d. Souza Jr, F. M. Silva, J. A. Chaker, P. A. Z. Suarez, *Ind Crop*
5 *Prod* **2014**, 59, 260.
- 6 [50] A. L. Drummond, N. C. Feitoza, G. C. Duarte, M. J. A. Sales, L. P. Silva, J. A. Chaker,
7 A. F. Bakuzis, M. H. Sousa, *J Nanosci Nanotechnol* **2012**, 12, 8061.
- 8 [51] E. F. B. Aransiola, E.; Layokun, S.K.; Solomon, B.O.;, *Int. J. Biol. Chem. Sci.* **2010** 4.
- 9 [52] A. Campanella, C. Fontanini, M. A. Baltanás, *Chemical Engineering Journal* **2008**, 144,
10 466.
- 11 [53] S. S. Bunker, C.; Willenbacher, N.; Wool, R.;, *Int. J. Adhes. Adhes.* **2003**, 23, 29.
- 12 [54] A. M. M. S. Medeiros, F. Machado, J. C. Rubim, T. F. L. McKenna, *Journal of Polymer*
13 *Science Part A: Polymer Chemistry* **2017**, 55, 1422.
- 14 [55] O. N. Shebanova, P. Lazor, *J Solid State Chem* **2003**, 174, 424.
- 15 [56] I. Chamritski, G. Burns, *J Phys Chem B* **2005**, 109, 4965.
- 16 [57] D. L. A. de Faria, S. Venâncio Silva, M. T. de Oliveira, *J Raman Spectrosc* **1997**, 28,
17 873.
- 18 [58] M. H. Sousa, F. A. Tourinho, J. C. Rubim, *J Raman Spectrosc* **2000**, 31, 185.
- 19 [59] A. L. Patterson, *Phys Rev* **1939**, 56, 978.
- 20 [60] C. Pereira, A. M. Pereira, C. Fernandes, M. Rocha, R. Mendes, M. P. Fernández-García,
21 A. Guedes, P. B. Tavares, J.-M. Grenèche, J. P. Araújo, C. Freire, *Chem Mat* **2012**, 24, 1496.
- 22 [61] Y. L. Mikhlin, A. V. Kuklinskiy, N. I. Pavlenko, V. A. Varnek, I. P. Asanov, A. V.
23 Okotrub, G. E. Selyutin, L. A. Solovyev, *Geochimic Cosmochim Ac* **2002**, 66, 4057.
- 24 [62] G. V. M. Jacintho, A. G. Brolo, P. Corio, P. A. Z. Suarez, J. C. Rubim, *The Journal of*
25 *Physical Chemistry C* **2009**, 113, 7684.
- 26 [63] K. Nakamoto, "*Infrared and Raman Spectra of Inorganic and Coordination*
27 *Compounds.*", Wiley, New York, 1986.
- 28 [64] J. A. R. M. n. Guivar, A. I.; Anaya, A. O.; Valladares, L. LS.; Félix, L. L.; Dominguez,
29 A. B.;, *Adv. in Nanoparticles* **2014**, 3, 114.
- 30 [65] I. Nurdin, M. R. Johan, I. I. Yaacob, B. C. Ang, A. Andriyana, *Mater Res Innov* **2014**,
31 18, S6.
- 32 [66] L. S. Laurentino, A. M. M. S. Medeiros, F. Machado, C. Costa, P. H. H. Araújo, C.
33 Sayer, *Chemical Engineering Research and Design* **2018**, 137, 213.
- 34 [67] X. Yang, S. Zhang, W. Li, *Progress in Organic Coatings* **2015**, 85, 216.
- 35 [68] B. Issa, I. Obaidat, B. Albiss, Y. Haik, *International Journal of Molecular Sciences* **2013**,
36 14, 21266.

37

1 **Tables**

2

3 Table 1

4

5 Table 1. Loadings of chemicals used in the miniemulsion polymerizations

Experiment	Styrene (g)	AFAME (g)	AIBN (g)	Hexadecane (g)	τ_{SPION} (wt.%) [*]
1	10	0	0.2	0.6	10
2	9.5	0.5	0.2	0.6	10
3	7.5	2.5	0.2	0.6	10
4	5	5	0.2	0.6	10

6 * τ = SPIONs content based on the total oil phase.

7

8 Table 2

9

10 Table 2. Tentative vibrational assignment for the IR absorptions observed in the spectra of

11 Figure 2

Wavenumber (cm ⁻¹)	Tentative assignment	Spectrum
573	Fe-O	(b) and (c)
1415	$\nu_s(\text{COO}^-)$	(c)
1462	$d(\text{CH}_2)^{[62]}$	(a)
1517	$\nu_{as}(\text{COO}^-)$	(c)
1624	$\delta(\text{O-H})$	(b)
1722	C=O	(a) and (c) [*]
2890	$\nu_s(\text{CH})$	(a) and (c)
2930	$\nu_{as}(\text{CH}_2)$	(a) and (c)
3010	$\nu(=\text{C-H})$	(a) and (c)
3400	$\nu(\text{OH})$	(b) and (c)

12 *non coordinated OA.

13

14 Table 3

15

16 Table 3. Data for calculating quantity of monolayers of OA on SPIONs-surface

	d/cm	$\rho/\text{g}\cdot\text{cm}^{-3}$	MM/g·mol ⁻¹	mass/g	$A_{\text{SPIONs}}/\text{cm}^2$	$A_{\text{OA}}/\text{cm}^2$
$\gamma\text{-Fe}_2\text{O}_3$	6.3×10^{-7}	4.9	-	7.33×10^{-3}	1.42×10^4	-
OA	-	-	282.5	1.83×10^{-3}	-	3.9×10^4

17

18

19

1 Table 4

2

3 Table 4. Particle size determined by DLS measurements

Experiment	Styrene/AFAME (wt%/wt%)	Particle size (nm)	PdI*
1	95/5	129	0.13
2	75/25	123	0.12
3	50/50	149	0.13

4 * The PdI is a value provided by Malvern instrument and it is used to describe the
5 width of the particle size distribution around a central value.

6

7 Table 5

8

9 Table 5. Experimental glass transition temperatures (T_g) of the magnetic and non-magnetic
10 samples determined by DSC/DTA

Non-Magnetic samples		Magnetic samples	
Sample	T_g (°C)	Sample	T_g (°C)
PolyAFAME	-55,4	-	-
Polystyrene	104	-	-
Poly(styrene ₉₅ - <i>co</i> -AFAME ₅)	51.2	poly(styrene ₉₅ - <i>co</i> -AFAME ₅)/ γ -Fe ₂ O ₃	61.7
Poly(styrene ₇₅ - <i>co</i> -AFAME ₂₅)	24.7	poly(styrene ₇₅ - <i>co</i> -AFAME ₂₅)/ γ -Fe ₂ O ₃	37.9
Poly(styrene ₅₀ - <i>co</i> -AFAME ₅₀)	-9.9	poly(styrene ₅₀ - <i>co</i> -AFAME ₅₀)/ γ -Fe ₂ O ₃	-4.8

11

12 Table 6

13

14 Table 6. Magnetization saturation (M_s), remanence (M_r) and coercivity (H_c) of poly(styrene-
15 *co*-AFAME)/ γ -Fe₂O₃ composites

Initial Composition (Styrene/AFAME) (wt%)	M_s (emu·g ⁻¹)	M_r (emu·g ⁻¹)	H_c (kOe)
95/5	41.5	0.1	0.002
75/25	31.5	0.01	3.6x10 ⁻⁴
50/50	26.2	0.02	3.3x10 ⁻⁴

17

18

19

20

21

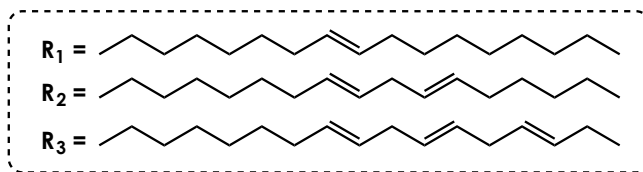
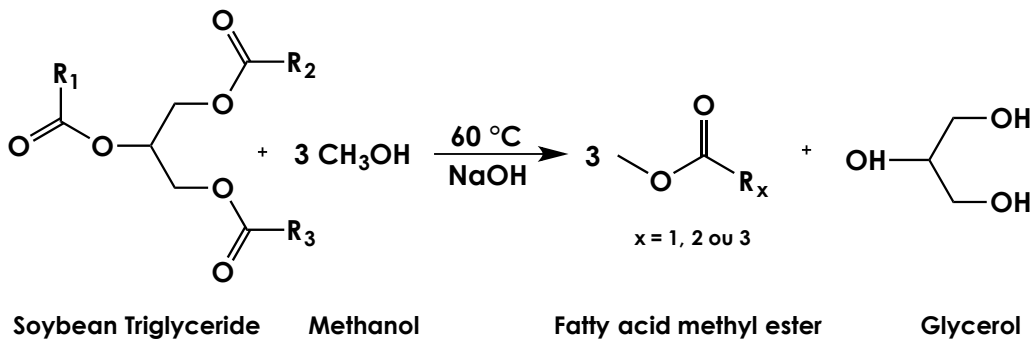
22

23

1 **Figures**

2

3 Figure 1

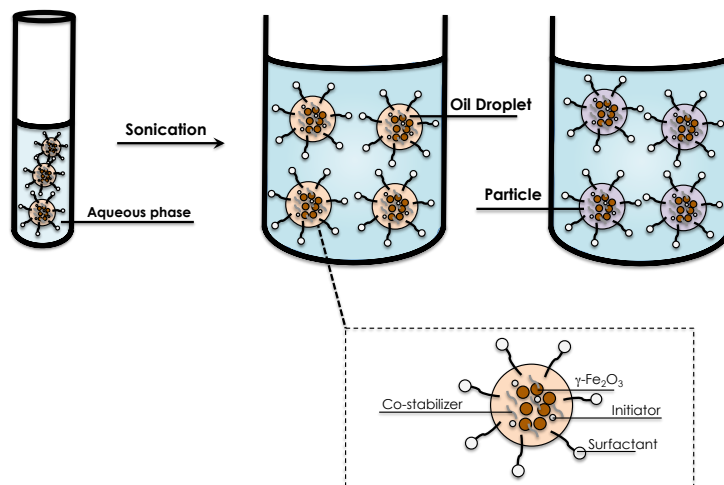


4

5

6 Figure 2

7



8

9

10

11

12

13

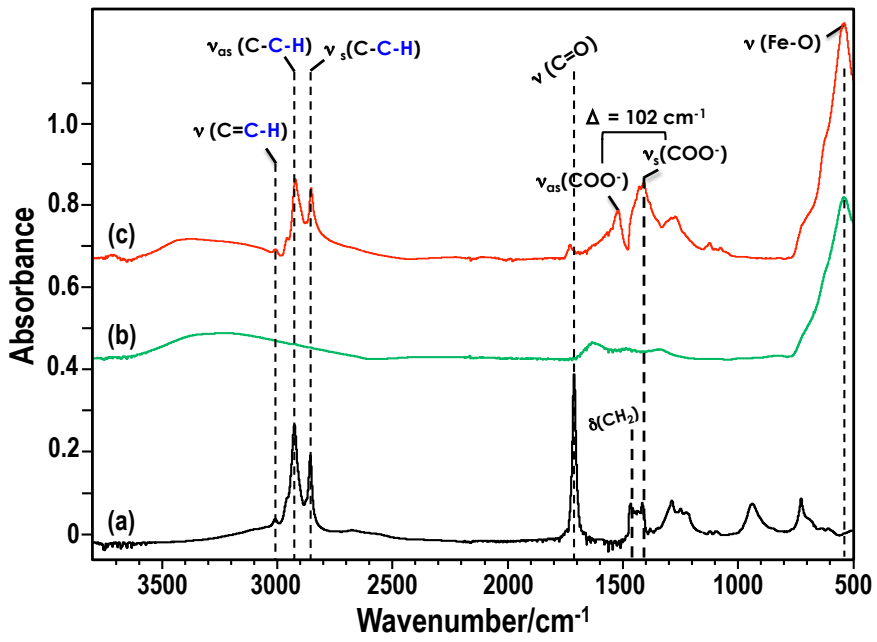
14

15

16

1 Figure 3

2

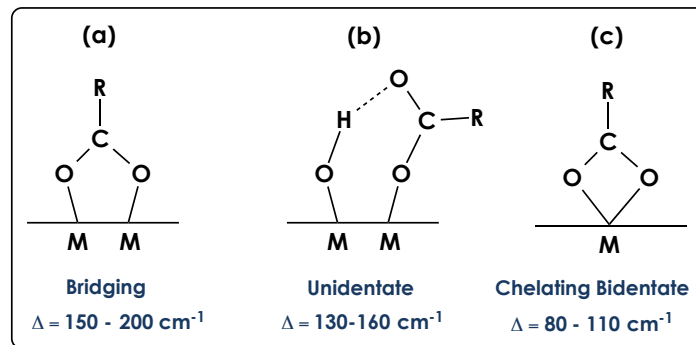


3

4

5 Figure 4

6



7

8

9

10

11

12

13

14

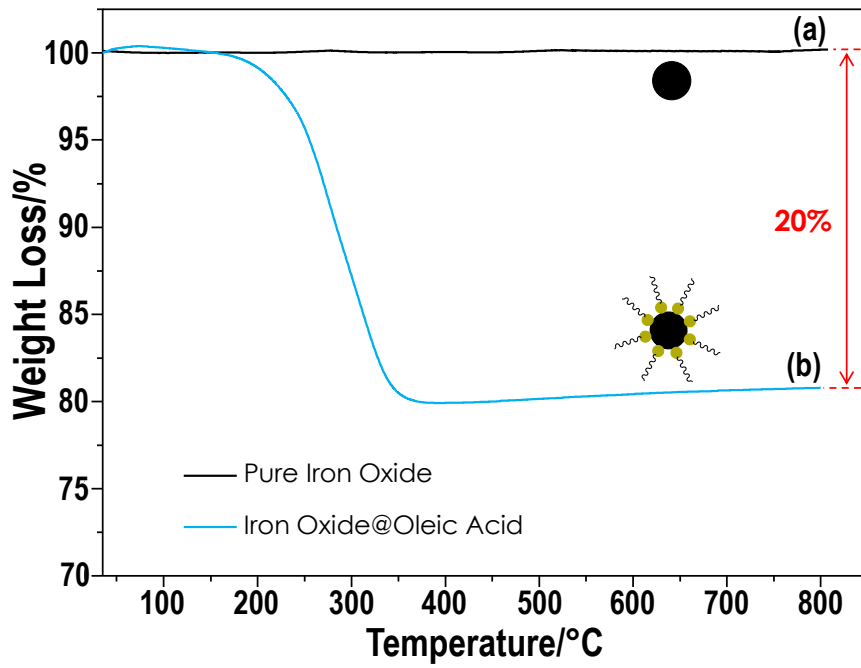
15

16

17

1 Figure 5

2

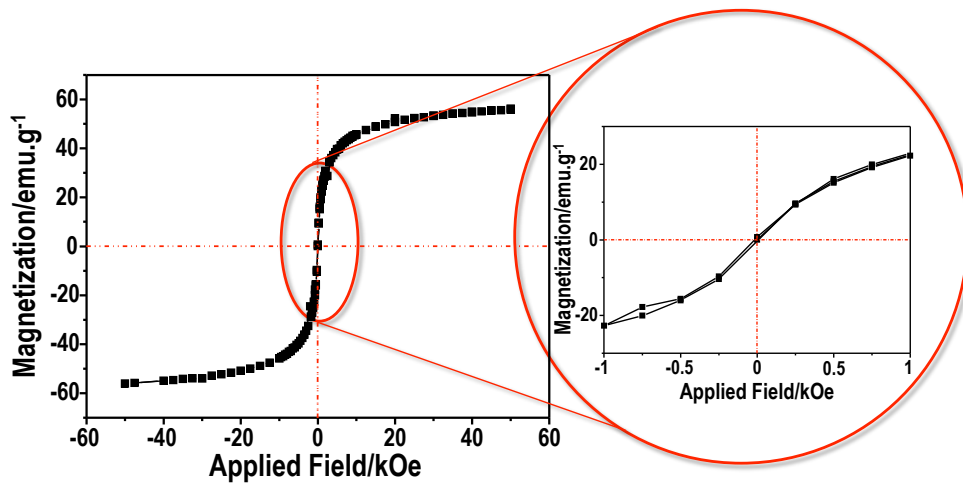


3

4

5 Figure 6

6



7

8

9

10

11

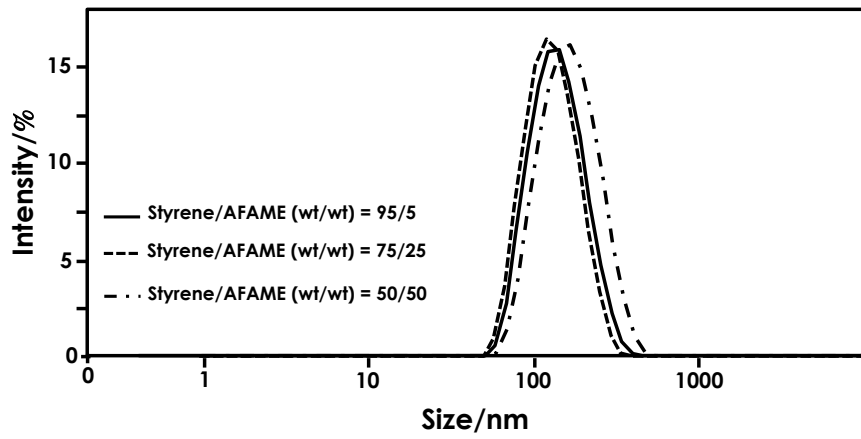
12

13

14

1 Figure 7

2

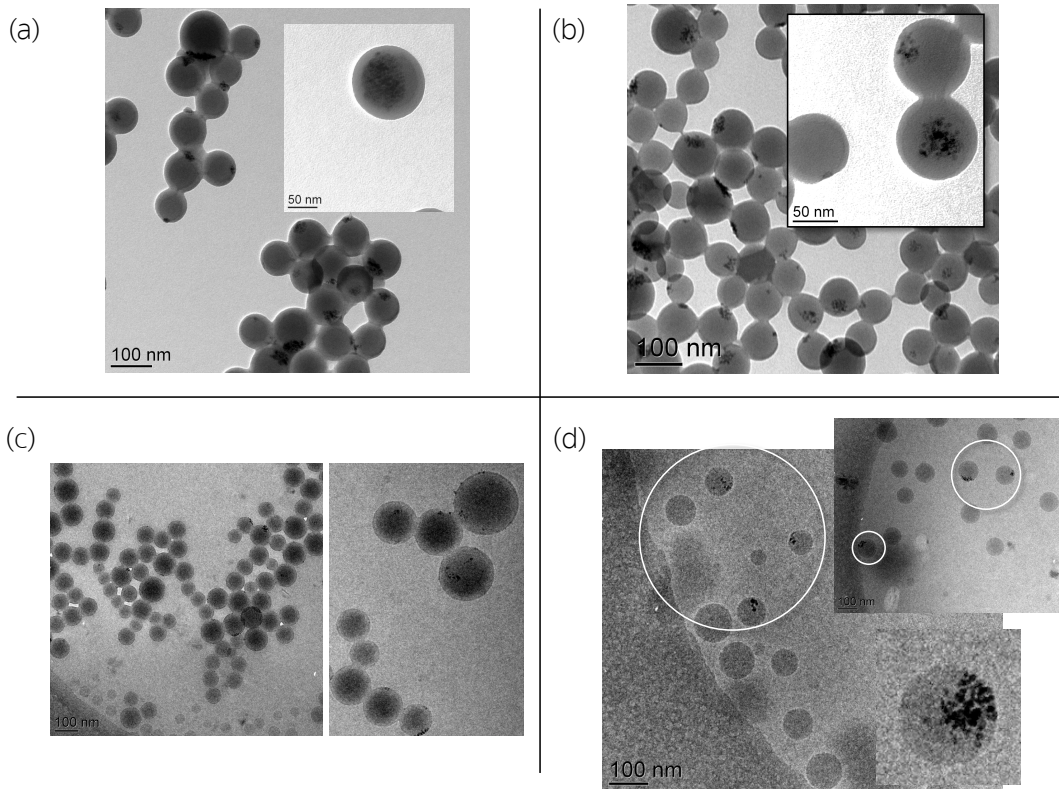


3

4

5 Figure 8

6



7

8

9

10

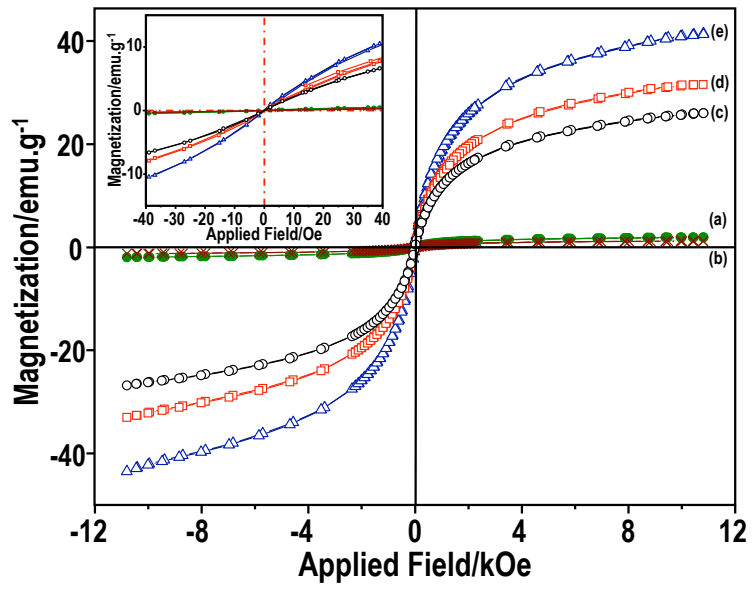
11

12

13

1 Figure 9

2

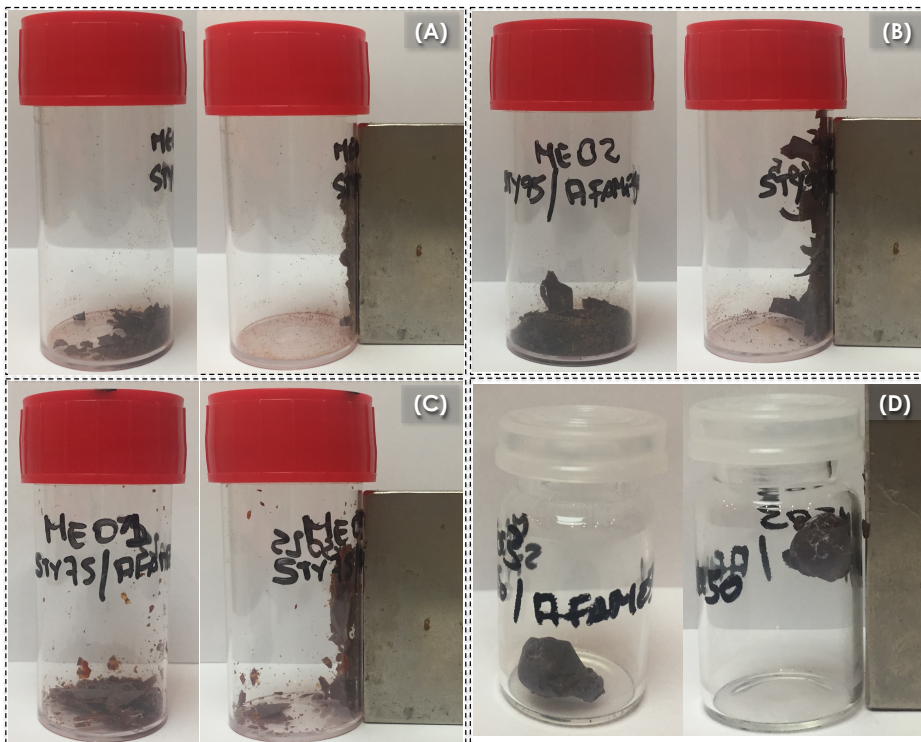


3

4

5 Figure 10

6



7

8

9

10

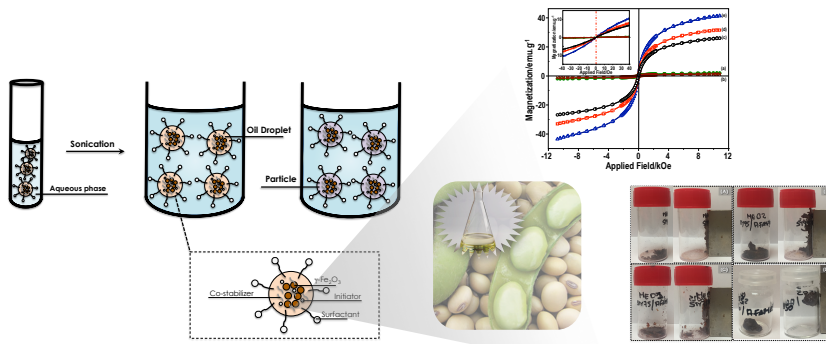
11

1 Table of Contents

2

3 The biomonomer obtained from soybean oil was used for the synthesis of bio-based hybrid
4 magnetic particles poly(styrene-co-AFAME)/ γ -Fe₂O₃ by miniemulsion polymerization. As
5 principal strategy, the superparamagnetic iron oxide nanoparticles γ -Fe₂O₃ were encapsulated
6 into styrene/AFAME-based copolymer matrix. The properties of poly(styrene-co-AFAME)/
7 γ -Fe₂O₃ can be modulated depending on its use by varying the amount of AFAME.

8



9